MICRO ION FREQUENCY STANDARD

P. D. D. Schwindt, R. Olsson, K. Wojciechowski, D. Serkland, T. Statom, H. Partner, G. Biedermann, L. Fang, A. Casias, and R. Manginell
Sandia National Laboratories
P.O. Box 5800, Albuquerque, NM 87185, USA

Abstract

We are developing a highly miniaturized trapped ion clock to probe the 12.6 GHz hyperfine transition in the $^{171}Yb^{+}$ ion. The clock development is being funded by the Integrated Micro Primary Atomic Clock Technology (IMPACT) program from DARPA, where the stated goals are to develop a clock that consumes 50 mW of power, has a size of 5 cm^3, and has a long-term frequency stability of 10^{-14} at 1 month. Trapped ion systems are an excellent candidate for such extreme miniaturization, because ions are well isolated from the environment independently of the size of the trap. Trapped ion clocks are characterized by quality factors, Q, in excess of 10^{12} and excellent long-term stability, and the Q will be minimally degraded upon miniaturization.

To realize the clock in a small package will require the miniaturization of several technologies. One of the primary technologies will be the miniaturized ion trap and vacuum package. Linear RF Paul traps routinely have dimensions of a couple millimeters, but miniaturizing the vacuum package with an integral trap, Yb source, and pump will require a novel design. Integrating the miniature, low-power light sources for state detection at 369 nm and 935 nm and for photoionization at 399 nm will also be critical. The 369 nm laser will be a frequency-doubled vertical external cavity surface-emitting laser (VECSEL). A low-phase-noise local oscillator at 12.6 GHz will also be developed using a micro resonator based on exciting acoustic resonances in aluminum nitride. We will present our proposed approach to developing the micro ion frequency standard and relevant current results.

INTRODUCTION

Vapor cell atomic clocks have seen extreme miniaturization within the past decade [**1**], and the success of such efforts has motivated research into the miniaturization of primary standards. Shifts due to the buffer gas used in the miniature vapor cells limit the accuracy and long-term stability of the clock [**2**]. To achieve high accuracy and long-term stability in a small package, the atoms must be extremely well isolated from the environment during interrogation with the microwave field. Our approach to achieving this isolation is to contain ions in a miniaturized ion trap. Surrounding the trap will be a miniature vacuum package, small low-power light sources, a local oscillator (LO), and control electronics.

Our choice of ion was limited to elements with nuclear spin of 1/2 and an electronic ground state of $S_{1/2}$. The ground state then contains the $F = 0$ and $F = 1$ hyperfine levels, where the $F = 0$ level contains only a single state (Figure 1(a)). State preparation to the $F = 0$, $m_F = 0$ is simplified in this case, because only optical pumping between hyperfine levels is required and not between Zeeman levels. For the miniaturized clock, we chose $^{171}Yb^{+}$, whose hyperfine ground state splitting is 12.6 GHz. A compact $^{199}Hg^{+}$ ion clock developed at the Jet Propulsion Laboratory has demonstrated a long-term stability at the

level of 10^{-16} while occupying a volume of ~1 liter [**3**]. Despite the excellent performance and relatively small size of this clock, we chose to design our clock around Yb, since the transition for optical pumping and state detection is at 369 nm, which can be accessed by a small, low-power frequency-doubled diode laser. The use of the laser light source also allows the state detection to occur with a cycling transition such that thousands of photons per ion are scattered. With the lamp-based Hg clock, one-two photons per ion are scattered.

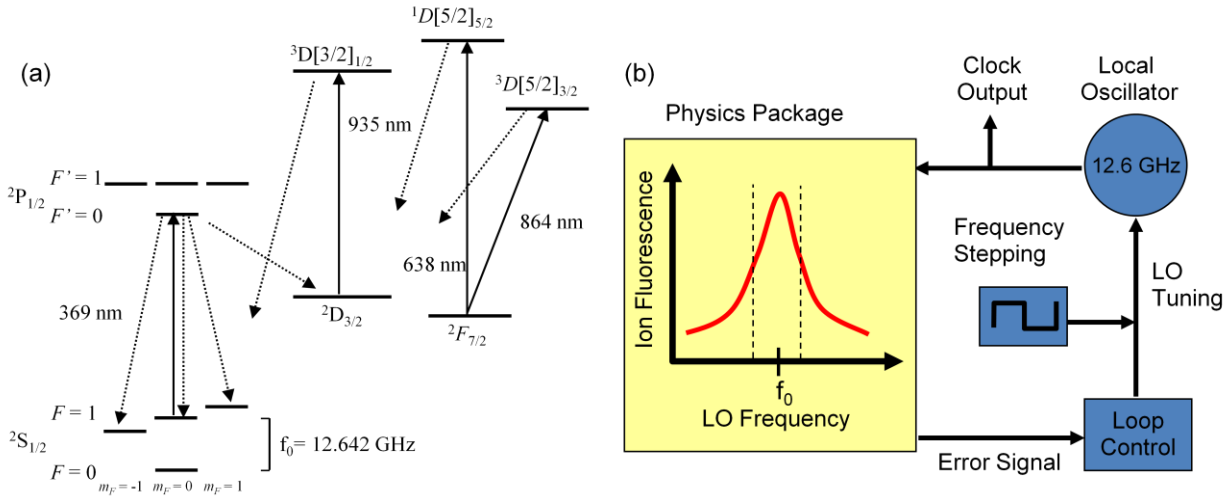

Figure 1. (a) Relevant energy level diagram of the $^{171}Yb^+$ ion showing the 12.6 GHz clock transition, the optical transitions. (b) System level schematic of the frequency control loop of the clock. The amplitude of the frequency stepping is adjusted to sample the maximum slope of the resonance, as indicated by the dashed lines.

Ytterbium has the additional complication of having low-lying $D_{3/2}$ and $F_{7/2}$ states. Decay from the $P_{1/2}$ state to the $D_{3/2}$ state has a branching ratio of 250:1, and the lifetime of the $D_{3/2}$ state is 53 ms [**4**]. To do efficient state detection and optical pumping, this state must be cleared out, which is typically done with a 935 nm laser. We are planning to explore the use of vertical cavity surface-emitting lasers (VCSELs) or light-emitting diodes (LEDs) for this purpose. Decay to the $F_{7/2}$ state is a rare event, and buffer gas cooled ions have been observed to decay to this state with a time constant of ~1 hour [**5**]. We will evaluate several strategies to clear this level, including optical pumping transitions at 638 nm or 864 nm, back filling with a N_2 buffer gas, and dumping and reloading the trap.

We plan to run the clock in the single-pulse mode where the 12.6 GHz microwave field from a local oscillator is pulsed on and off to drive a π-pulse from the $F = 0$, $m_F = 0$ to the $F = 1$, $m_F = 0$. To determine how many ions made the transition, the 369 nm and the 935 nm light fields illuminate the ions, and the ion fluorescence from the $F = 1$ to the $F' = 0$ transition is collected on a detector. The detector signal is conditioned in loop-control electronics to generate a control signal to lock the frequency of the LO to the ion hyperfine transition (Figure 1(b)). The state detection process also serves to optically pump the ion back to the $F = 0$ state. As the ions are optically pumped out of the $D_{3/2}$, they can decay to either ground state. The performance goal for this clock is to achieve an Allan variance of $2 \times 10^{-11}\ \tau^{-1/2}$. When trapping 10^5 ions, the shot-noise-limited stability would be more than an order of magnitude better than the goal with a microwave interrogation time of 100 ms. However, we expect detector inefficiencies, laser noise, and LO noise to be technical challenges to achieving the required performance.

ION TRAP AND VACUUM PACKAGE

Central to the micro ion frequency standard is the miniature vacuum package (Figure 2). At a minimum, the package must contain the ion trap, a Yb source, and a getter pump. The Yb source will be constructed from a micromachined silicon hotplate that has Yb evaporated onto the surface. The getter pump will maintain the required vacuum inside the package, which is 10^{-6} torr of a He or Ne buffer gas with the partial pressures of other gases a few orders of magnitude lower. The buffer gas provides a cooling mechanism for the trapped ions. We envision the trap to be an integral part of the vacuum package to minimize the overall size of the package. Figure 3 shows a package that could be fabricated from either high-temperature or low-temperature co-fired ceramic. The co-fired ceramics have electrical traces and vias integrated into the layers of the ceramic, allowing for an easily configured package. The ion trap is a linear rf Paul trap in an octupole configuration. Bonding pads are arrayed in layers within the package so that gold wires can be stretched across a span and bonded with a deep access wire bonder to form the rf electrodes. Endcap electrodes are formed by running wires perpendicular to the rf electrodes. The wires and the package are arranged to allow optical access along the longitudinal axis of the trap freeing up the other axes for fluorescence collection and the Yb source.

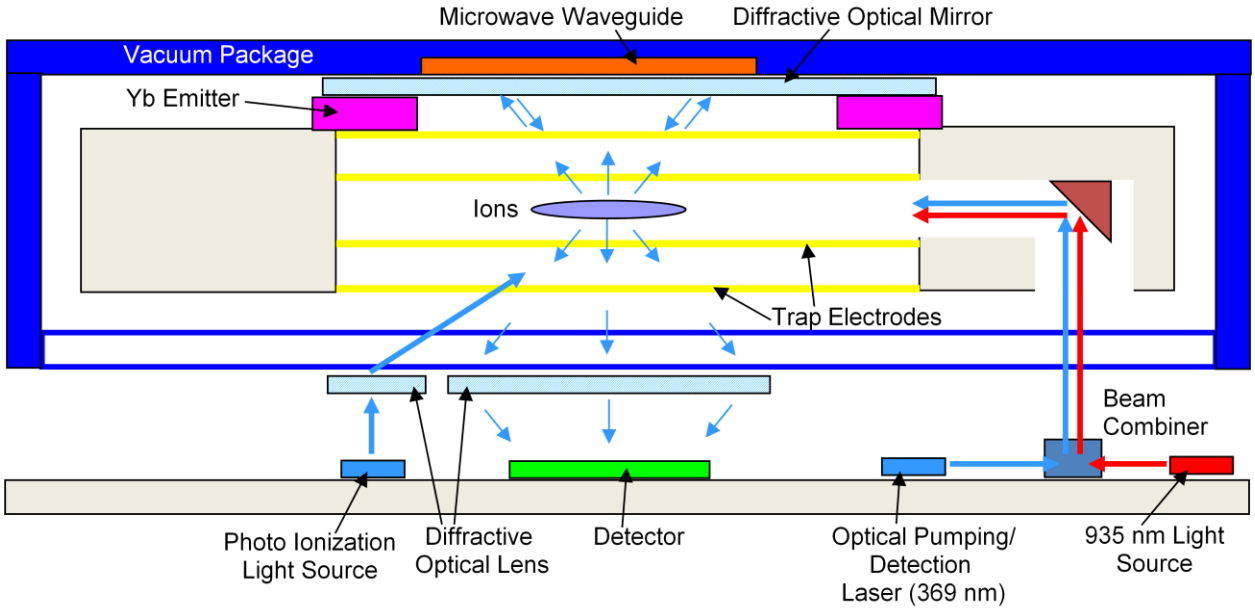

Figure 2. Schematic drawing of the vacuum package and octupole ion trap with integrated components. A magnetic shield would surround the vacuum package.

The octupole geometry was chosen for the ion trap to balance good optical access and large trap depth against one of the largest systemic shifts in ion clocks, the second-order Doppler shift. The second-order Doppler shift arises from the motion of the ions to which there are two components: the thermal motion of the ions and the micromotion caused by the rf trapping potential. The shift due to the micromotion can be minimized by increasing the number of poles (radial electrodes) providing the radial confinement [**6**]. Higher pole traps form steep-walled potentials maximizing the volume within the trap free from micromotion. Due to ion-ion repulsion, increasing the number of ions in the trap forces more ions to the edges of the trap, increasing the micromotion. In our trap, we expect a shift of 8×10^{-15} for a 40% change in ion number when trapping 10^6 ions. By using the octupole trap, we reduce the optical access to the

ions. To maximize the optical access, we plan to use gold wires with a width of ~100 μm, while the trap radius is 1-1.5 mm. The small electrodes reduce the depth of the trap by a factor of 10 compared to an ideal octupole. Nevertheless, we can achieve a depth of 1.5 eV by applying a 2 MHz voltage with an amplitude of 75 V.

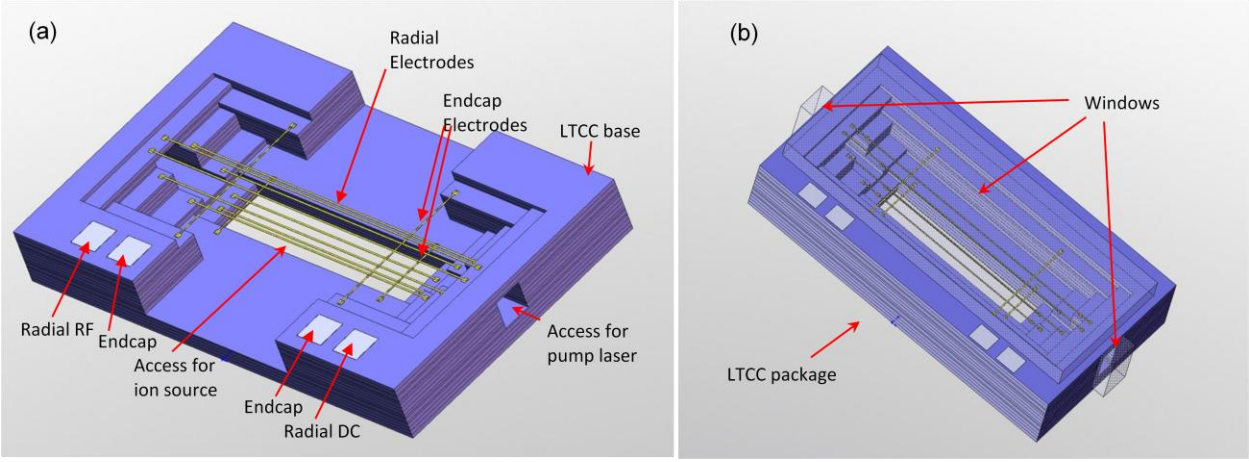

Figure 3. (a) Drawing of the octupole ion trap formed from low temperature co-fired ceramic (LTCC). (b) Drawing of a fully sealed LTCC package where the windows would be sealed on with a solder, braze, or sealing glass.

To create ions in the trap, we plan to investigate two methods: electron impact ionization and photo ionization. Electron impact ionization is inefficient and readily charges up dielectric surfaces that will be in close proximity to the trap in the small vacuum package. This may combine with the potential required to accelerate the electrons to significantly reduce the depth of the trap. In addition, the electrons can ionize contaminants in the vacuum package or the buffer gas, resulting in unwanted trapped species. In photo ionization, neutral Yb is ionized with two photons, one at 399 nm and another at <394 nm. Photo ionization is much more efficient, does not have the charging issues, and can only ionize Yb, but it requires a laser source at 399 nm, which may be difficult in a small package with no locking reference. We will explore doubled diode lasers and LEDs as potential light sources.

We are currently building an experimental test bed to study the issues surrounding the miniaturization of the trapped ion clock. In the test bed, we plan to demonstrate trapping and clock operation in an octupole trap made with gold wire and low-temperature co-fired ceramic, to study the different ionization techniques and ways to depopulate the *F*-state, and to test other miniaturized system components, such as the LO and 369 nm laser, prior to integration. We are now trapping ions in a conventional vacuum chamber with a linear quadrupole trap, and plan to demonstrate a clock in the coming months to prove the functionality of the test bed.

LOCAL OSCILLATOR

The local oscillator (LO) is one of the primary components limiting the overall stability of the Micro Ion Frequency Standard. Not only is the short-term stability of the oscillator in Figure 1 set by the LO, but the minimum bandwidth of the loop control that locks the LO to the hyperfine transition is set by the LO

stability to noise and temperature. As the LO stability is increased, the interrogation time of the hyperfine transition can be increased, raising the effective Q of the trapped ions and improving the ion clock frequency stability. The short-term performance of the clock in terms of the Allan deviation is given by

$$\sigma_y(\tau) = \frac{1}{2T_R\nu_0}\sqrt{\frac{T_c}{\tau}}\frac{1}{S/N} \qquad (1)$$

where τ is the averaging time, T_R is the interrogation time of the hyperfine transition of the ions, ν_0 is the atomic hyperfine resonance frequency, T_c is the cycle time, and S/N is the signal to noise ratio of the fluorescence detection. In Figure 4, the blue curves represent the fractional frequency stability of the LO, exhibiting $1/f^2$ phase noise, for various LO resonator quality factors (Q) and resonator powers of 1 mW, well within the linear operating region of the proposed LO resonator. The red line in Figure 4 represents the stability limit due to a fixed dead time of T_c - T_R = 50 ms and T_R is varied. Where the LO stability intersects the red line is approximately the time constant at which the control loop transfers the stability of the ions to the local oscillator. The green curves in Figure 4 represent the limit due to τ which is the stability of the trapped ions inside the bandwidth of the control loop in Figure 1. Finally, the black line in Figure 4 represents the IMPACT Phase III stability goal. As can be seen in Figure 4, to achieve the IMPACT goals requires an LO with a minimum fractional frequency stability at 60 ms of 80 parts-per-trillion (ppt) and a resonator minimum loaded Q of 150. This, however, assumes ideal stability performance from the ions. A more realistic goal for the LO to achieve the IMPACT metrics is a fractional frequency stability of 8 ppt at 100 ms, requiring a resonator Q of 1,450 at 12.6 GHz.

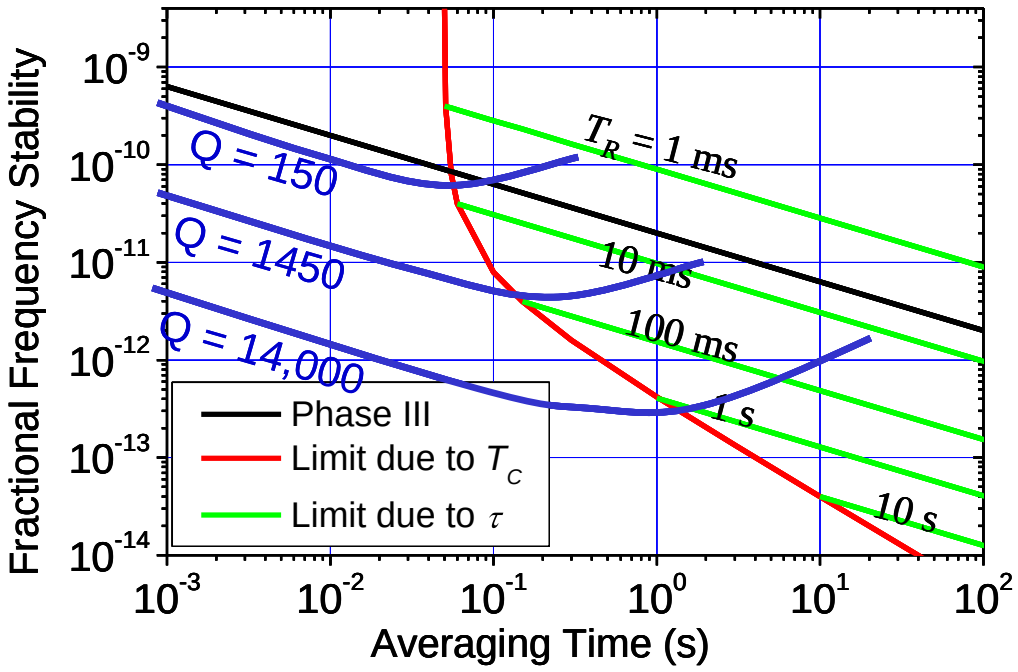

Figure 4. Fractional frequency stability limit of the trapped ion clock for various LO resonator quality factors and hyperfine transition interrogation times.

Due to the small volume and power requirements, we have chosen to directly synthesize our LO at 12.6 GHz rather than upconverting a low-frequency low-phase-noise temperature stable LO to 12.6 GHz. This gives two main advantages. First, only one oscillator is required for the LO, saving size and power. Second, since temperature compensation through resonator ovenization is required to increase LO stability and trapped ion interrogation time, ovenizing a miniature 12.6 GHz resonator can be done in a fraction of the power of ovenizing a large low-frequency resonator, for example a 10 MHz quartz crystal.

We plan to base our LO on a 12.6 GHz aluminum nitride (AlN) μresonator. A picture of an AlN plate μresonator fabricated using the simple two-mask process in [**7**] is shown in Figure 5(a). Through proper layout of the electrodes, the thickness mode in the plate can be transduced via laterally spaced electrodes included only on top of the resonator. Using only top electrodes simplifies fabrication complexity and increases the overall resonant frequency. The measured response of a laterally transduced thickness mode resonator operating at 13.25 GHz is shown in Figure 5(b). The resonator exhibits an unloaded quality factor of 510, above that required to meet the IMPACT metrics (150) and approaching the desired value of 1450. The theoretical Q limit of AlN at 12.6 GHz is 1600. The frequency of this resonator can be reduced to 12.6 GHz by increasing the thickness of the 300 nm AlN plate in Figure 5.

An AlN or other acoustic resonator cannot be manufactured to sub part-per-billion (ppb) accuracy, and a free-running AlN based oscillator cannot maintain sub-ppb stability over drift, noise, and temperature. Further investigation of the resonator in Figure 5(a) reveals empty areas on the plate where micro-ovens and temperature sensors can be deployed. Since AlN resonators have a temperature coefficient of frequency that can be engineered from -30 to +10 parts-per-million (ppm) per degree C [**8**], our plan is to utilize the micro-oven to thermally tune the resonator to the hyperfine transition using the control loop in Figure 1. Once the LO has been thermally tuned to the hyperfine transition, the micro-oven can be used to temperature-stabilize the resonator around 12.6 GHz to increase the ion interrogation time. A major challenge will be engineering the thermal and electrical interconnects to the resonator to minimize oven power consumption.

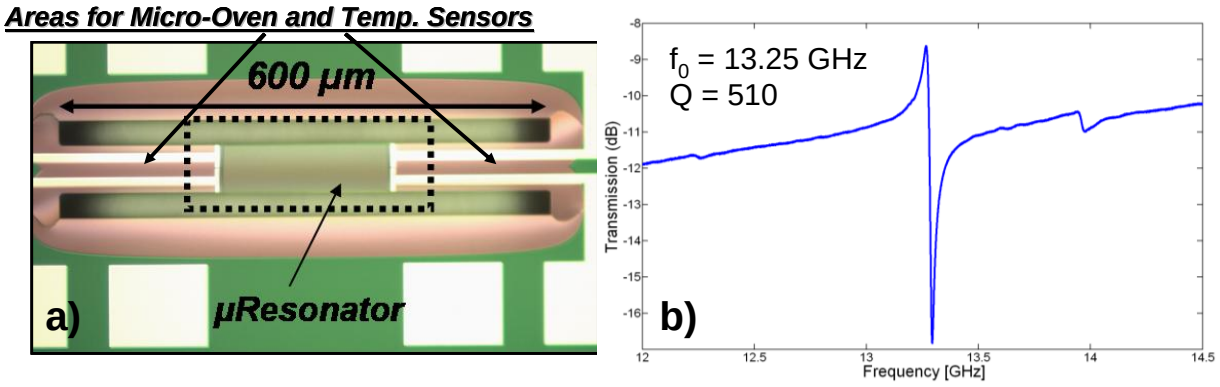

Figure 5. Laterally excited thickness mode plate resonator and measured response.

FREQUENCY-DOUBLED DIODE LASER

We have chosen to produce the 369 nm light source, used for excitation of the Yb ions, by frequency-doubling a low-power vertical-cavity surface-emitting laser (VCSEL) operating at 738 nm. Although a 369 nm laser diode could be made using GaN-based semiconductor materials, similar to commercially

available 405 nm laser diodes, the power consumption of currently available 405 nm diode lasers is too high to fit within the ultimate 10 mW power budget available for the laser used in this atomic clock. In contrast, VCSELs in the 800-nm wavelength range typically reach threshold at drive levels below 2 mW of power and they can readily achieve efficiencies above 30%. Since only 20 μW of power is required at 369 nm, a low frequency-doubling conversion efficiency of 0.5% is adequate, given 4 mW of VCSEL power available at 738 nm. Still, achieving even 0.5% frequency-doubling efficiency is not trivial with only 4 mW of fundamental-frequency power, since nonlinear conversion efficiencies scale with input power. The two most promising nonlinear crystals for frequency-doubling to 369 nm are periodically poled lithium tantalate (PPLT) and periodically poled potassium titanyl phosphate (PPKTP). In order to achieve the required conversion efficiency, the nonlinear crystal must either be placed inside a high-finesse resonant optical cavity or be used in a waveguide configuration that maintains high optical field intensity over a long interaction length.

We have grown a few 738-nm VCSEL wafers by metal-organic chemical-vapor deposition (MOCVD) and fabricated lasers as shown in Figure 6(a). As shown by the emission spectrum in Figure 6(b), a 3-μm-aperture is sufficiently small to obtain single-transverse-mode operation at 738 nm. We employed 8-nm-thick $Al_{.16}Ga_{.84}As$ quantum wells to yield optical gain at 738 nm. The distributed Bragg reflectors (DBRs) are composed of $Al_{.34}Ga_{.66}As$ and $Al_{.92}Ga_{.08}As$ as the high- and low-index layers, respectively, with compositional grades between them to minimize the series resistance of the DBRs.

(a)

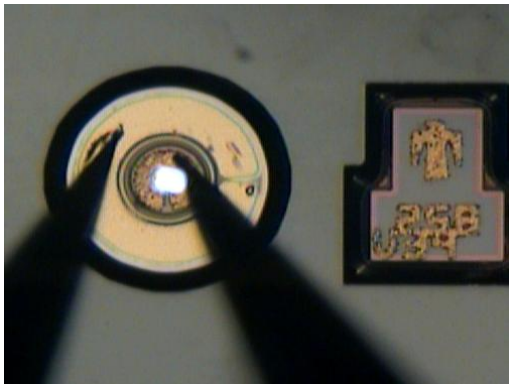

(b)

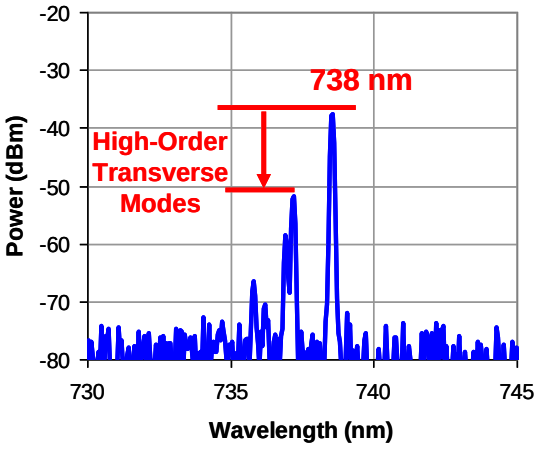

Figure 6. (a) Fabricated VCSEL. (b) Emission spectrum of VCSEL at 1 mA drive current.

As expected, our initial VCSEL wafers produced much less output power than the ultimate 4 mW goal, as shown in Figure 7(a). Although further optimization of the epitaxial semiconductor materials may improve the output power somewhat, we plan to pursue a vertical-*external*-cavity surface-emitting laser (VECSEL) as a means to both increase the output power by extracting power from a larger area of the semiconductor wafer and simultaneously narrow the linewidth due to a longer photon lifetime in the laser cavity. The challenge with the VECSEL is to retain the low threshold power consumption and relatively high conversion efficiency of a regular VCSEL, while maintaining operation in a single longitudinal, transverse, and polarization mode.

Finally, a picture of a PPKTP waveguide chip made by AdvR is shown in Figure 7(b). Ultimately, we require a conversion efficiency of 1.25×10^{-3} mW^{-1} to convert from 4 mW at 738 nm to 20 μW at 369

nm. The current waveguide chip achieves conversion efficiencies of approximately 0.25 × 10^{-3} mW^{-1}, suggesting that further development of nonlinear devices will be required to meet out ultimate power goals. Nevertheless, it seems clear that combining a low-power VCSEL at 738-nm with a nonlinear frequency-doubling device is a viable path to produce the required fluorescence excitation light source at 369 nm.

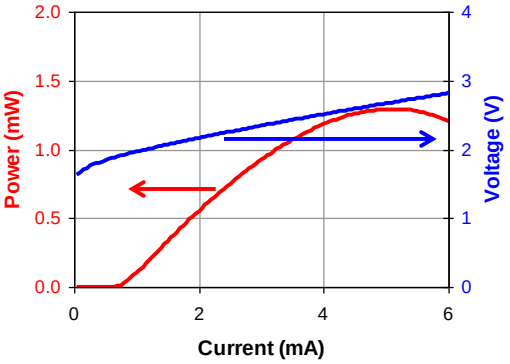

(a)

(b)

Figure 7. (a) 740-nm VCSEL output power and voltage versus current. (b) Periodically poled KTP crystal with patterned waveguides for frequency-doubling to 369 nm.

CONCLUSION

Developing a micro ion frequency standard will require the miniaturization and integration of several key technologies. Miniaturizing and reducing power consumption of the trap and vacuum package, the LO, and the 369 nm laser will be the thrust of the initial phase of the research. Research in later phases will include integration of the components with small, low-power control electronics and further miniaturization. An atomic clock that consumes 50 mW of power, has a size of 5 cm^3, and has a long-term frequency stability of 10^{-14} at 1 month would be a revolutionary advance in atomic clock technology, opening up new applications in navigation, communication, and timing.

REFERENCES

[**1**] R. Lutwak, A. Rashed, D. K. Serkland, G. M. Peake, M. Varghese, G. Tepolt, J. R. Leblanc, M. Mescher, 2007, *"The miniature atomic clock – pre-production results,"* in Proceedings of the IEEE International Frequency Control Symposium (FCS) and 21st European Frequency and Time Forum (EFTF), 29 May-1 June 2007, Geneva, Switzerland (IEEE CFP07FRE), pp. 1327-1333; S. Knappe, V. Shah, P. D. D. Schwindt, L. Hollberg, J. Kitching, L. Liew, and J. Moreland, 2004, *"A microfabricated atomic clock,"* **Applied Physics Letters, 85,** 1460-1462.

[**2**] S. Knappe, V. Gerginov, P. Schwindt, V. Shah, H.G. Robinson, L. Hollberg and J. Kitching, 2005, *"Atomic vapor cells for chip-scale atomic clocks with improved long-term frequency stability,"* **Optics Letters, 30**, 2351-2353.

[**3**] J. D. Prestage and G L. Weaver, 2007, *"Atomic clocks and oscillators for deep-space navigation and radio science,"* **Proceedings of the IEEE, 95,** 2235-2247.

[**4**] S. Olmschenk, K. C. Younge, D. L. Moehring, D. N. Matsukevich, P. Maunz, and C. Monroe, 2007, *"Manipulation and Detection of a Trapped Yb+ Hyperfine Qubit,"* **Physical Review A, 76**, 052314.

[**5**] P. T. H. Fisk, M. J. Sellars, M. A. Lawn, and C. Coles, 1995, *"Performance of a prototype microwave frequency standard based on laser-detected, trapped $^{171}Yb^{+}$ ions,"* **Applied Physics B, 60,** 519-527.

[**6**] J. D. Prestage, R. L. Tjoelker, and L. Maleki, 2000, *"Mercury-Ion Clock Based on Linear Multi-Pole Ion Trap,"* in Proceedings of the IEEE/EIA International Frequency Control Symposium and Exhibition, 7-9 June 2000, Kansas City, Missouri, USA (IEEE 00CH37052), pp. 706-710.

[**7**] K. E. Wojciechowski, R. H. Olsson III, *et al*., 2009, *"Super High Frequency Width Extensional Aluminum Nitride MEMS Resonators,"* in Proceedings of the IEEE Ultrasonics Symposium, 20-23 September 2009, Rome, Italy, in press.

[**8**] R. H. Olsson, C. M. Washburn, J. E. Stevens, M. R. Tuck, and C. D. Nordquist, 2008, "*VHF and UHF mechanically coupled aluminum nitride MEMS filters,"* in Proceedings of the IEEE International Frequency Control Symposium (FCS) and PDA Exhibition, 19-21 May 2008, Honolulu, Hawaii, USA (IEEE CFP08FRE), pp. 634-639.